

Chapter 1

General Basics

This introductory chapter provides the basics for this book, and terms such as micrometeorology, atmospheric boundary layer, and meteorological scales are defined and presented in relation to the subject matter of this book. Besides an historical outline, the energy and water balance equations at the Earth's surface and the transport processes are discussed. The first chapter of the book focus on the micrometeorological basics, which are then expanded in the following theoretical and experimental chapters.

1.1 Micrometeorology

Meteorology is one of the oldest sciences in the world. It can be traced back to Aristotle (384–322 BCE), who wrote the four volumes of the book *Meteorology*. In ancient times, appearances in the air were called meteors. In the first half of the 20th century, the upper soil layers were considered part of meteorology (Hann and Süring 1939). Today meteorology is understood in a very general sense to be the science of the atmosphere (Glickman 2000; Dutton 2002; Kraus 2004), and includes also the mean states (climatology). Sometimes the definition of meteorology is very narrow, and only related to the physics of the atmosphere or weather prediction. To understand atmospheric processes, many other sciences such as physics, chemistry, biology and all geosciences are necessary, and it is not easy to find the boundaries of these disciplines. In a pragmatic way, meteorology is related only to processes that take place in situ in the atmosphere, while other sciences can investigate processes and reactions in the laboratory. This underlines the specific character of meteorology, i.e., a science that investigates an open system with a great number of atmospheric influences operating at all times but with changing intensity. Meteorology is subdivided into branches (Houghton 1985; Glickman 2000; Kraus 2004; Hupfer and Kuttler 2005). The main branches are theoretical meteorology,

observational meteorology, and applied meteorology. Applied meteorology includes weather prediction and climatology. Climatology must be seen in a much wider geosciences context. The subdivision is continued up to special areas of investigation such as maritime meteorology.

The applications of time and space scales became popular over the last 50 years, and subdivisions into macro-, meso- and micrometeorology were developed. Micrometeorology is not restricted to particular processes, but to the time and space scales of these processes (see Sect. 1.2). The significance of micrometeorology is in this limitation. The living environment of mankind is the main object of micrometeorological research. This is the atmospheric surface layer, the lowest 5–10% of the atmospheric boundary layer, which ranges in depth from about 0.5–2 km.

The surface layer is one of the main energy-exchange layers of the atmosphere, and accordingly the transformations of solar energy into other forms of energy are a main subject of micrometeorology. Furthermore, the surface layer is a source of friction, which causes a dramatic modification of the wind field and the exchange processes between the Earth's surface and the free troposphere. Due to the coupling of time and space scales in the atmosphere, the relevant time scale of micrometeorology is less than the diurnal cycle. A recent definition of micrometeorology is (Glickman 2000):

Micrometeorology is a part of Meteorology that deals with observations and processes in the smaller scales of time and space, approximately smaller than 1 km and one day. Micrometeorological processes are limited to shallow layers with frictional influence (slightly larger phenomena such as convective thermals are not part of micrometeorology). Therefore, the subject of micrometeorology is the bottom of the atmospheric boundary layer, namely, the surface layer. Exchange processes of energy, gases, etc., between the atmosphere and the underlying surface (water, soil, plants) are important topics. Microclimatology describes the time-averaged (long-term) micrometeorological processes while the micrometeorologist is interested in their fluctuations.

If one examines the areas of investigation of applied meteorology (Fig. 1.1) it will be apparent that the main topics are related to microscale processes (Houghton 1985). Therefore, we see that micrometeorology gives the theoretical, experimental, and climatological basis for most of the applied parts of meteorology, which are related to the surface layer and the atmospheric boundary layer. Also, recent definitions such as environmental meteorology are related to micrometeorology. Applied meteorology often includes weather prediction and the study of air pollution.

The basics of micrometeorology come from hydrodynamics and in particular the dynamics of turbulent flow. An interesting overview about the history of the science of turbulence is given by Davidson et al. (2011). The following historical remarks are based on papers by Lumley and Yaglom (2001), Foken (2006), and Davidson

Applied Meteorology						
Hydro meteo- rology	Technical Meteorology			Biometeorology		
	Construc- tion Meteoro- logy	Traffic Meteo- rology	Industrial Meteo- rology	Agricultural Meteoro- logy	Forest Mete- orology	Human Biometeoro- logy
		Transport Meteo- rology		Phenology		

Fig. 1.1 Classification of applied meteorology

et al. (2011). The origin may be dated to the year 1895, when Reynolds (1894) defined the averaging of turbulent processes, and described the equation of turbulent energy. Further steps were the mixing length approach by Taylor (1915) and Prandtl (1925), and the consideration of buoyancy effects by Richardson (1920). The every-day term ‘turbulence element’ is based on Barkov (1914), who found these in wind observations analyzed during a long stay in winter in the Antarctic ice shield. The actual term *micrometeorology* is dated to the determination of energy and matter exchange and the formulation of the *Austausch coefficient* by Schmidt (1925) in Vienna. At the same time in Munich, Geiger (1927) summarized microclimatological works in his famous book *The Climate near the Ground*, which is still in print (Geiger et al. 2009; Geiger 2013). The experimental and climatological application of these investigations of turbulent exchange processes were done mainly by Albrecht (1940) in Potsdam, who also wrote parts of the classical textbook by Kleinschmidt (1935) on meteorological instruments. Furthermore, Lettau (1939, translation into English 1944 in USA) investigated the turbulence near the surface and the atmospheric boundary layer in Leipzig and continued his investigation after the Second World War in the U.S.A. (Lettau and Davidson 1957). With the end of the Second World War, an era of more than 20 years of famous German-speaking micrometeorological scientists ended, but the word *Austausch coefficient* was maintained from that period on.

The origin of modern turbulence research in micrometeorology was in the 1940s in Russia. Following the fundamental studies on isotropic turbulence and the turbulence spectra by Kármán and Howardt (1938) and Taylor (1938), Kolmogorov (1941a, b) gave theoretical reasons for the turbulence spectra. In 1943, Obukhov (published in 1946), found a scaling parameter that connects all near-surface turbulence processes. This paper (Obukhov 1971) was so important because of its relevance to micrometeorology, it was once again published by Businger and Yaglom (1971). A similar paper was published by Lettau (1949), but was not applied because it used a different scaling. Using what became known as *Monin-Obukhov*

similarity theory, Monin and Obukhov (1954) created the basics of the modern stability-dependent determination of the exchange process. At the same time, a direct method to measure turbulent fluxes was developed (Montgomery 1948; Obukhov 1951; Swinbank 1951), which has become known as the *eddy-covariance* method. This method became truly established only after the development of the sonic anemometer, for which the basic equations were given by Schotland (1955). Following the development of a sonic thermometer by Barrett and Suomi (1949), a vertical sonic anemometer with 1 m path length (Suomi 1957) was used in the O'Neill experiment in 1953 (Lettau and Davidson 1957). The design of today's anemometers was first developed by Bovscheverov and Voronov (1960), and later improved by Kaimal and Businger (1963) and Mitsuta (1966). These first anemometers used the phase shift method between the transmitted and the received signal or the difference in the travel time between the transmitter and receiver as the signal travels in both directions. Recent anemometers directly measure the travel times in both directions along each path (Hanafusa et al. 1982). Following the early work by Sheppard (1947), the surface stress was directly measured with a drag plate in Australia (Bradley 1968), and the sensible and latent heat fluxes were measured with highly sensitive modified classical sensors (Dyer et al. 1967).

The new theoretical concepts and sensor developments formed the basis for many famous experiments (see Appendix A.5). Among them were the many prominent Australian experiments for studying turbulent exchange processes (Garratt and Hicks 1990), and the so-called intercomparison experiments for turbulence sensors (Miyake et al. 1971; Tsvang et al. 1973; Dyer et al. 1982; Tsvang et al. 1985). Present day parameterizations are primarily based on the KANSAS 1968 experiment (Izumi 1971; Kaimal and Wyngaard 1990). That experiment became the basis for the formulation of the universal functions (Businger et al. 1971) and the turbulence energy equation (Wyngaard et al. 1971), which were based on an earlier, not well-known paper by Obukhov (1960). Twenty years after the issue of the first textbook on micrometeorology by Sutton (1953), an important state-of-the-art summary of turbulent exchange between the lower atmosphere and the surface was given in 1973 at the *Workshop on Micrometeorology* (Haugen 1973).

After some criticism of the experimental design of the KANSAS experiment by Wieringa (1980), and the reply by Wyngaard et al. (1982), who recommended a repetition of the experiment, several micrometeorological experiments were conducted, including investigations of fundamental micrometeorological issues, for example the Swedish experiments at Lövsta (Högström 1990). Finally, the corrected universal functions by Högström (1988) comprise our most current knowledge.

At the end of the 1980s, the step to micrometeorological experiments in heterogeneous terrain became possible. At about the same time, similar experiments were conducted in the U.S.A. (FIFE, Sellers et al. 1988), in France (HAPEX, André et al. 1990) and in Russia (KUREX, Tsvang et al. 1991). These experiments were to become the bases of many further experiments (see Appendix A.5). A number of experiments, often equipped with an extensive suite of instruments, focused on

investigating particular atmospheric processes, such as turbulent fluxes in an heterogeneous landscape (LITFASS-2003, Beyrich and Mengelkamp 2006), energy exchange above ice and snow in the Arctic (SHEBA, 1997/98, Persson et al. 2002), stable stratification (CASES-99, Poulos et al. 2002), energy balance closure (EBEX-2000, Oncley et al. 2007), convective boundary layer processes (COPS 2007, Wulfmeyer et al. 2011), or boundary layer processes in the late afternoon (BLLAST 2011, Lothon et al. 2014).

During the last 40 years, significant progress has been made in the theoretical understanding of surface-layer processes and in the development of precision instruments. As a result, the number of available data sets has increased significantly, but scientific breakthroughs for a more realistic treatment of phenomena such as heterogeneous surfaces or stable boundary layers are still missing.

1.2 Atmospheric Scales

Contrary to other geophysical processes, meteorological processes have a clear time-space scaling (Beniston 1998). The reason for this is the spectral organization of atmospheric processes, where relevant wavelengths (extensions) are related to distinct durations in time (frequencies). The largest wavelengths are those of atmospheric circulation systems with 3–6 days duration and an extension of some thousands of kilometers (macro-turbulence, Rossby waves). The daily cycle is a prominent frequency. The time interval from minutes to seconds is characterized by exchange processes of energy and matter in the range of the so-called micro-turbulence, a main topic of micrometeorological investigations (see Sect. 1.4.3). The intermediate range, called meso-turbulence, is an area of relatively low energy (Etling 2008) that includes also local circulation systems. The principle of classification was formulated by Orlanski (1975), see Fig. 1.2. While atmospheric processes are strictly organized, the hydrological processes in soils and plant ecosystems have for the same time scales significantly smaller space scales. It is possible to define an “ecological gap” between single-plant or chamber measurements and the micrometeorological measurements, which are related to a footprint with a spatial dimension of about 50–100 m. For example, in the case of coupling hydrological or ecological with atmospheric models one must develop strategies to transfer the small-scale processes to the larger atmospheric space scale.

Different scale definitions in different scientific disciplines create problems in interdisciplinary communications. In addition, in climatology textbooks different scale concepts are discussed which are not easily comparable with the very clear meteorological scale concepts (see Sect. 7.1).

Because weather phenomena are classified according to space-time scales, the space-time scales of climate and weather prediction models must be classified in a similar way. For example, large-scale circulation models are assigned to the macro- β range. The classical weather forecast was formally related to the meso- α range,

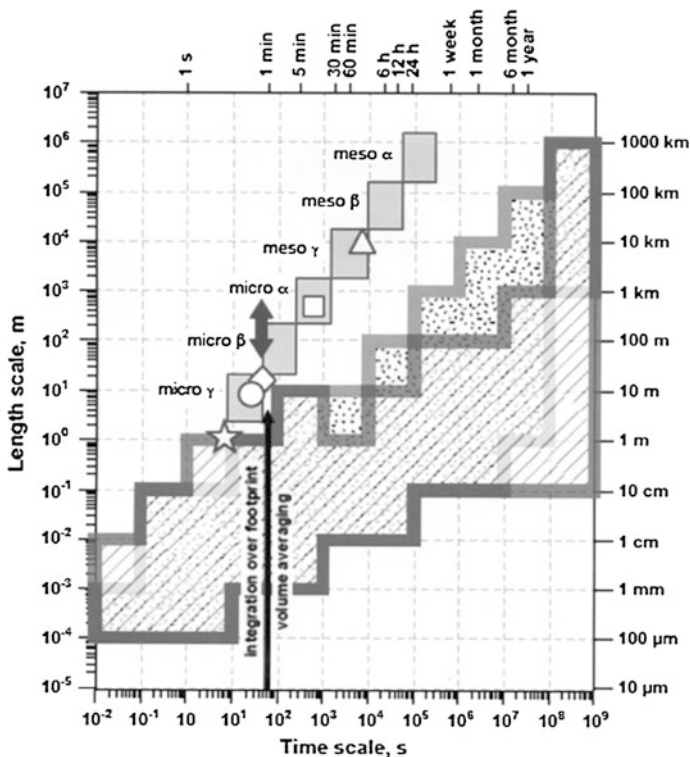


Fig. 1.2 Temporal and spatial scales of atmospheric (turbulent), biospheric (physiological) and soil processes. Atmospheric processes (Orlanski 1975) are *light grey* quadrats in the size of one scale (von micro γ bis meso α) shown. The scales of the plant processes, relevant for the energy and matter exchange with the atmosphere (Schoonmaker 1998) are shown as the speckled area and the soil processes (Blöschl and Sivapalan 1995; Vogel and Roth 2003) as hatched area (Foken et al. 2012, modified). Additionally, shown are (see following chapters): transport processes in tall forest canopies that comprise turbulent transport inside canopies (*star*), vertical advection inside canopies (*circle*), turbulent transport above canopies (*diamond*), coherent structures (*double arrow*), footprint averaged turbulent fluxes (*square*), and horizontal advection at the canopy top (*triangle*). Chemical reactions can be related to relevant scales by volume averaging (with kind permission of © Author(s) 2012. CC Attribution 3.0 License, All rights reserved)

but with today's high-resolution models they are related to the meso- β, γ scale. Micrometeorology is related to all micro-scales and also partly to the meso- γ scale.

This scaling principle is basic for measurements of atmospheric processes. For instance, to measure the spatial extension of a small low-pressure system, high-resolution (small scale) measurements are necessary, which are often not available in operational meteorological networks. The same is true for the movement of systems. The frequency of these measurements must be related to the velocity of the pressure system. This is valid for all scales, and phenomena can only be observed if the measurements are made on smaller space and time scales.

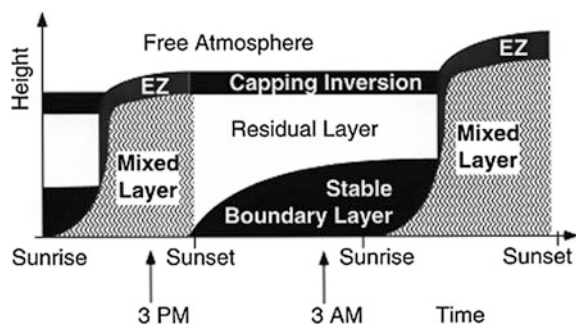
Therefore, the sampling theorem (see Sect. 6.1.2) is of prime importance for all meteorological measurements and scales. It is also possible to postulate a “technical sensing gap” between the typical range of the footprint (50–100 m) of meteorological measurements and the smallest size of grid cells of most of the conventional models or of polar circulating satellites (see Sect. 6.2).

1.3 Atmospheric Boundary Layer

The atmospheric boundary layer is the lowest part of the troposphere near the ground where the friction stress decreases with height. The wind velocity decreases significantly from its geostrophic value above the boundary layer to the wind near the surface, and the wind direction changes counter-clockwise up to 30–45° in the Northern hemisphere. In addition, thermal properties influence the boundary layer (Stull 1988; Kraus 2008). Frequently the synonym *planetary boundary layer* is used in theoretical meteorology, where the general regularities of the boundary layers of planetary atmospheres are investigated. Above the boundary layer, lays a mostly statically-stable layer (inversion) with intermittent turbulence. The exchange processes between the atmospheric boundary layer and the troposphere take place in the entrainment zone. The thickness of this layer is approximately 10% of the atmospheric boundary layer, which has a thickness of about 1–2 km over land and 0.5 km over the oceans. For strong stable stratification, its thickness can be about 10 m or less.

The daily cycle is highly variable (Stull 1988), see Fig. 1.3. After sunrise, the atmosphere is warmed by the turbulent heat flux from the ground surface, and the inversion layer formed during the night brakes up. The new layer is very turbulent, well mixed (mixed layer), and bounded above by an entrainment zone. Shortly before sunset, the stable (night time) boundary layer develops near the ground. This stable layer has the character of a surface inversion. Above this layer, remnants of the daytime mixed layer linger but turbulence, but turbulence is much weaker in this so called residual layer. It is capped by a free (capping) inversion—the upper border of the boundary layer (Seibert et al. 2000). After sunrise, the developing

Fig. 1.3 Daily cycle of the structure of the atmospheric boundary layer, EZ Entrainment zone (published with kind permission of © Prof. Roland Stull, Vancouver, All rights reserved)



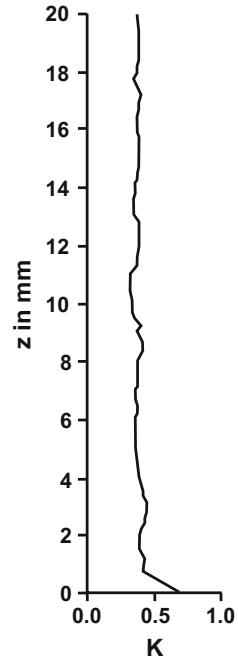
Height in m	Name		Exchange		Stability
1000	Upper layer (Ekman-layer)		Turbulent	No const. flux	Influence of stability
20	Turbulent layer	Surface layer (Prandtl-layer)		Flux constant with height	
	Roughness sublayer				
1	Dynamical sublayer			Molecular/turbulent	
0.01	Viscous sublayer				Molecular
0.001	Laminar boundary layer				
				No influence of stability	

Fig. 1.4 Structure of the atmospheric boundary layer

mixed layer quickly destroys the stable boundary layer and the residual layer. On cloudy days and in winter, when the solar radiation and the energy transport from the surface to the atmosphere are weak, the mixed-layer development will be damped, and characteristics of the previous day boundary layer may persist throughout the day. On days with strong solar radiation, the nocturnal boundary-layer structure quickly vanishes as convective cells develop at about 10 m above the ground over areas with strong sensible heat fluxes. These convective cells, have narrow areas of strong updrafts surrounded by broader regions of weaker downdrafts. According to model studies, these convective cells develop over areas which are larger than 200–500 m (e.g. Shen and Leclerc 1995).

In the upper part of the atmospheric boundary layer (upper layer or Ekman layer), the changes of the wind direction take place. The lowest 10% is called the surface or Prandtl layer (Fig. 1.4). It is also called the *constant flux layer* because of the assumption of constant fluxes with height within the layer. This offers the possibility to estimate, for example, the fluxes of sensible and latent heat in this layer while in the upper layers flux divergences dominate. The atmospheric boundary layer is turbulent to a large degree, and only within a few millimeters above the surface do the molecular exchange processes dominate. Because the turbulent processes are about 10^5 -fold more effective than molecular processes and because of the assumption of a constant flux, the linear vertical gradients of properties very near the surface must be very large. For example, temperature gradients up to 10^3 K m^{-1} have been measured (Fig. 1.5). Between this molecular boundary layer (term used for scalars) or laminar boundary layer (term used for the flow field) and the turbulent layer, a viscous sublayer (buffer layer) exists with mixed exchange conditions and a thickness of about 1 cm. According to the

Fig. 1.5 Vertical temperature profile above a water surface with a molecular boundary layer, which has an linear temperature gradient (adapted from Foken et al. 1978 with kind permission of © Kluwer Academic Publisher B.V. Dordrecht 1978, All rights reserved)



similarity theory of Monin and Obukhov (1954), a layer with a thickness of approximately 1 m (dynamical sublayer) is not influenced by the atmospheric stability—this layer is nearly neutral all of the time. Above tall vegetation or buildings, the constant flux layer assumption is no longer fulfilled due to the high friction and the surface layer must be divided into additional layers. Immediately above the canopy up to roughly twice of the canopy height, in the so-called mixing layer or roughness sublayer (Garratt 1978), turbulent mixing is increased. If the vegetation is not too high, a surface layer may develop above the mixing layer but its thickness is reduced. Within the canopy layer the constant flux assumption is also not fulfilled; for more details see Sects. 3.1.3 and 3.5.

All processes in the atmospheric boundary layer, mainly in the micrometeorological range near the ground surface (nearly neutral stratification), can be compared easily with measurements made in the laboratory (wind tunnels and water channels). Thus, the research of the hydrodynamics of boundary layers at a wall, for example by Prandtl, is applicable to atmospheric boundary layer research (Monin and Yaglom 1973, 1975; Schlichting and Gersten 2003; Oertel 2004). As will be shown in the following chapters, knowledge in micrometeorology is based to a large extent on hydrodynamic investigations. In the wind tunnel, many processes can be studied more easily than in nature. But, the reproduction of atmospheric processes in the wind tunnel also means a transformation of all the similarity

numbers (see Sect. 2.1.2). Therefore, non-neutral processes can be studied in the laboratory only if extremely large temperature or density gradients can be realized in the fluid channels.

1.4 Energy Balance at the Earth's Surface

The earth's surface is the main energy transfer area for atmospheric processes (Fig. 1.6). It is heated by the shortwave down-welling irradiation from the sun ($K\downarrow$), and only a part of this radiation is reflected back ($K\uparrow$). Furthermore, the surface absorbs longwave down-welling radiation due to longwave emission by clouds, particles and gases ($I\downarrow$). The absorbed energy is emitted only partly into the atmosphere as longwave up-welling radiation ($I\uparrow$). In the total balance, the earth's surface receives more radiation energy than is lost, i.e. the net radiation at the ground surface is positive ($-Q_s^*$, see Sect. 1.4.1). The surplus of supplied energy will be transported back to the atmosphere due to two turbulent energy fluxes (see Sect. 1.4.3), the sensible heat flux (Q_H) and the latent heat flux (Q_E , evaporation). Furthermore, energy is transported into the soil due to the ground heat flux (Q_G) (see Sect. 1.4.2) and will be stored by plants, buildings, etc. (ΔQ_s). The sensible heat flux is responsible for heating the atmosphere from the surface up to some 100 m during the day, except for days with strong convection. The energy balance at the earth's surface according to the law of energy conservation (see also Sect. 3.7) is:

$$-Q_s^* = Q_H + Q_E + Q_G + \Delta Q_s \quad (1.1)$$

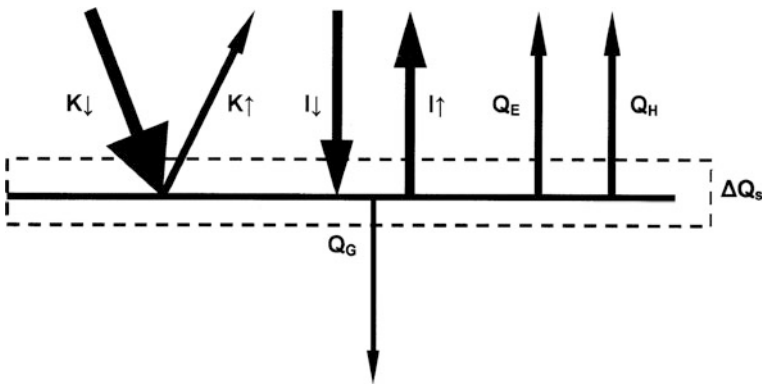


Fig. 1.6 Schematic diagram of the radiation and energy fluxes at the earth's surface. The net radiation according to Eq. (1.1) is the sum of the short-wave down-welling ($K\downarrow$) and reflected radiation ($K\uparrow$), and the long-wave radiation fluxes from the earth surface ($I\uparrow$) and from clouds, particles, and gases ($I\downarrow$). The energy balance is the sum of the net radiation, the sensible heat flux (Q_H), the latent heat flux (Q_E), and the ground heat flux (Q_G). In addition to the turbulent fluxes, the energy storage ΔQ_s in the air, in the plants, and in the soil are given

Supplement 1.1¹ Energy and radiation fluxes in meteorology

Energy and radiation-fluxes in meteorology are given in terms of densities. While the unit of energy is the Joule (J) and for power is Watt ($W = J s^{-1}$), the unit for the energy flux density is $W m^{-2}$. It appears that the energy flux density has *apparently* no relation to time, but the exact unit is $J s^{-1} m^{-2}$. To determine the energy that $1 m^2$ gets during 1 h, multiply the energy flux density by 3600 s. Energy fluxes expressed as $J m^{-2}$ are unusual in meteorology except daily sums which are given in $MJ m^{-2}$ (Mega-Joules per square meter), and sometimes kWh (kilo-Watt-hours).

Energy balance values are defined as radiation and energy flux densities (Bird et al. 2007) given in the dimension Wm^{-2} (Supplement 1.1). The following convention will be applied:

Radiation and energy fluxes are positive if they transport energy away from the earth's surface (into the atmosphere or into the ground), otherwise they are negative. The sign of the number gives the direction of the flux.

The advantage of this convention is that the turbulent fluxes and the ground heat flux are positive at noon. This convention is not used in a uniform way in the literature, e.g. in macro-scale meteorology the opposite sign is used. Often, all upward directed fluxes are assumed as positive (Stull 1988). In this case, the ground heat flux has the opposite sign of that given above. In other textbooks, the global radiation and the turbulent fluxes are shown with a positive sign in the figures (Oke 1987; Arya 2001), which makes the figures easier to read but can be confusing. The applied convention is identical with the presentations by Garratt (1992), because $-Q_s^* > 0$. In the end, the choice of the convention is not important, but the energy balance Eq. (1.1) must be fulfilled.

The components of the energy balance are shown in schematic form in Fig. 1.7. Remarkable is the high variation of the sensible and latent heat flux in comparison to the net radiation, which is a result of wind velocity changes. In the case of changing cloudiness, all terms become highly variable. The same variations occur in the case of some micrometeorological processes, which will be discussed in the following chapters. The most important variances are a positive latent heat flux after sunset and a negative sensible heat flux that begins in the early afternoon (oasis effect). A negative latent heat flux (evaporation) is identical with dewfall. The long-term mean values of the earth's energy balance are given in Table 1.1. Even

¹Supplements are short summaries from textbooks in meteorology and other sciences. These are included for an enhanced understanding of this book or for comparisons. For details, see the relevant textbooks.

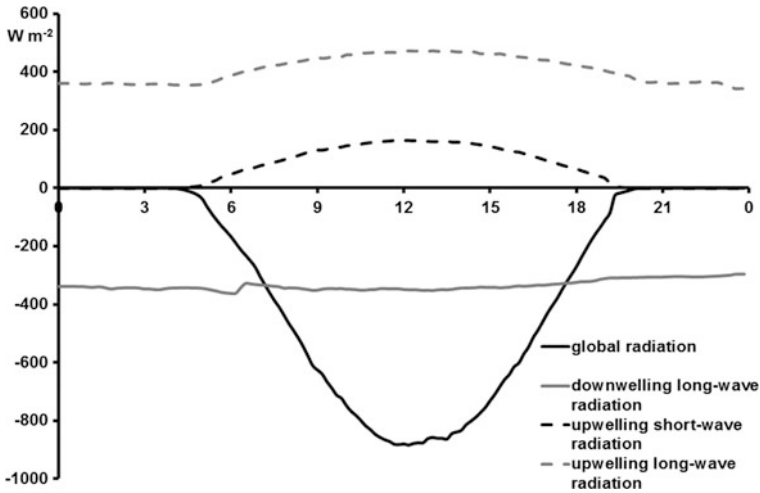


Fig. 1.7 Schematic of the daily cycle energy balance (May 24, 2012, Ecological-Botanical Garden of the University of Bayreuth, from Foken 2013 with kind permission from © Edition am Gutenbergplatz Leipzig 2013, All rights reserved)

Table 1.1 Radiation and energy fluxes in Wm^{-2} at the earth surface (Kiehl and Trenberth 1997, modified and updated)

Reference	$K_{\downarrow} - K_{\uparrow}$	$I_{\uparrow} - I_{\downarrow}$	Q_H	Q_E
Budyko (1974) ^a	-157	52	17	88
Henderson-Sellers and Robinson (1986) ^a	-171	68	24	79
Liou (1992) ^a	-151	51	21	79
Hartmann (1994) ^a	-171	72	17	82
Kiehl and Trenberth (1997) ^a	-168	66	24	78
Trenberth et al. (2009) ^b	-161	63	17	80
Wild et al. (2013) ^c , uncertainty	-161 (-154 ... -166)	56 (46 ... 62)	20 (15 ... 25)	84 (70 ... 85)
Wild et al. (2015) ^c , Land uncertainty	-136 (-132 ... -143)	34 (27 ... 39)	32 (25 ... 36)	38 (34 ... 45)
Wild et al. (2015) ^c , Ocean uncertainty	-170 (-174 ... -176)	53 (49 ... 57)	16 (11 ... 18)	100 (90 ... 105)

^aIrradiation at the upper boundary of the atmosphere 342 Wm^{-2}

^bIrradiation at the upper boundary of the atmosphere 341 Wm^{-2} , 1 Wm^{-2} at the earth surface absorbed

^cIrradiation at the upper boundary of the atmosphere 340 Wm^{-2} , 0.6 Wm^{-2} (uncertainty $0.2 \dots 1.0 \text{ Wm}^{-2}$) at the earth surface absorbed

though the values of the radiation fluxes are high, the radiation balance is relatively low with a value of about 100 Wm^{-2} . Noticeable is the inaccuracy of the turbulent fluxes, which, among other factors, can be explained by the difficulties in measuring and evaluation these terms. The 1 K increase of the global mean temperature in the last century due to anthropogenic greenhouse gas emissions corresponds to an additional radiation energy of 2 Wm^{-2} . Therefore, changes in the radiation and energy fluxes, e.g. due to changes in land use, can have significant effects on the climate system.

1.4.1 Net Radiation at the Earth's Surface

The radiation in the atmosphere is divided into shortwave (solar) radiation and longwave (heat) radiation. Longwave radiation has wavelengths $>3 \mu\text{m}$ (Supplement 1.2). The net radiation at the ground surface is given by:

$$Q_s^* = K \uparrow + K \downarrow + I \uparrow + I \downarrow \quad (1.2)$$

From Eq. (1.2) we see that the net radiation is the sum of the shortwave down-welling radiation mainly from the sun (global radiation), the longwave down-welling infrared (heat) radiation emitted by clouds, aerosols, and gases, the shortwave up-welling reflected (solar) radiation, and the longwave up-welling infrared (heat) radiation. The shortwave radiation can be divided into the diffuse radiation from the sky and direct solar radiation.

Table 1.1 gives the climatological-averages of the magnitudes of the components of the energy and radiation balance equation. These values are based on recent measurements of the mean solar incoming shortwave radiation at the upper boundary of the atmosphere (cross-section area of the earth πR^2 , R : radius of the earth), i.e. $S = -1361 \text{ Wm}^{-2}$ (Kopp and Lean 2011) in energetic units or -1.119 Kms^{-1} in kinematic units (for conversion between these units, see Sect. 2.3.1). Therefore, the daily average at the upper boundary layer of the atmosphere (surface of the globe $4\pi R^2$) is 340 Wm^{-2} . Figure 1.8 shows the typical daily cycle of the components of the net radiation. The ratio of reflected to the incoming shortwave radiation is called the albedo:

$$a = -\frac{K \uparrow}{K \downarrow} \quad (1.3)$$

In Table 1.2 the albedos for different surfaces are given.

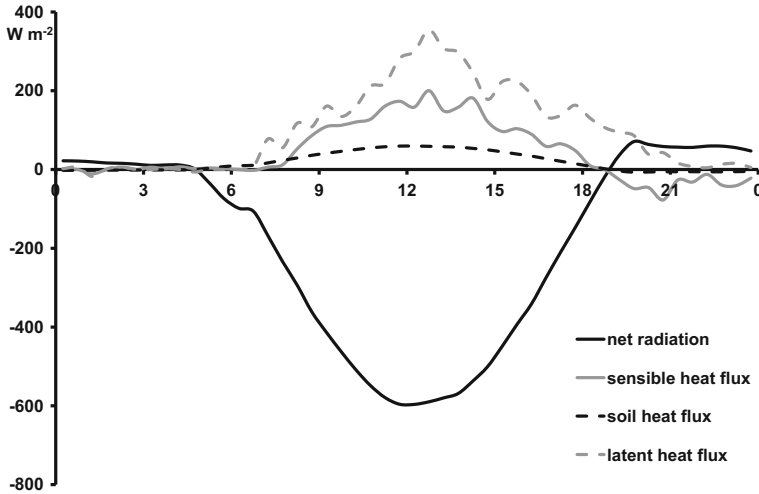


Fig. 1.8 Schematic of the diurnal cycle of the components of the net radiation (May 24, 2012, Ecological-Botanical Garden of the University of Bayreuth, from Foken 2013 with kind permission from © Edition am Gutenbergplatz Leipzig 2013, All rights reserved)

Table 1.2 Albedo of different surfaces (Geiger et al. 2009)

Surface	Albedo
Clean snow	0.75–0.98
Grey soil, dry	0.25–0.30
Grey soil, wet	0.10–0.12
White sand	0.34–0.40
Wheat	0.10–0.25
Grass	0.18–0.20
Oaks	0.18
Pine	0.14
Water, rough, solar angle 90°	0.13
Water, rough, solar angle 30°	0.024

The longwave radiation fluxes can be determined according to the Stefan-Boltzmann law:

$$I = \varepsilon_{IR} \sigma_{SB} T^4 \quad (1.4)$$

Supplement 1.2 Spectral classification of the radiation

Spectral classification of short and long wave radiation (Wendisch and Yang 2012, modified)

Notation	Wave length in μm	Remarks
<i>Ultraviolet radiation</i>		
UV-C-range	0.010–0.280	Does not penetrate the atmosphere
UV-B-range	0.280–0.315	Does partly penetrate the atmosphere
UV-A-range	0.315–0.370	Penetrates the atmosphere
<i>Visible radiation</i>		
Violet	0.370–0.455	
Blue	0.455–0.492	
Green	0.492–0.576	
Yellow	0.576–0.597	
Orange	0.597–0.622	
Red	0.622–0.680	
Dark red	0.680–0.750	
<i>Infrared radiation</i>		
Near infrared (NIR)	0.750–2.0	
Infrared (IR)	2.0–1000.0	

where the infrared emissivities for different surfaces are given in Table 1.3, and $\sigma_{SB} = 5.67 \cdot 10^{-8} \text{ W m}^{-2} \text{ K}^{-4}$ is the Stefan-Boltzmann constant.

In general, the up-welling longwave radiation is greater than the down-welling longwave radiation, because the earth’s surface is warmer than clouds, aerosols, and gases. It is only in the case of fog, that up-welling and down-welling radiation are equal. The down-welling radiation may be greater if clouds appear in a previously clear sky and the ground surface has cooled. Under clear sky without clouds and dry air, the radiation temperature is approximately $-55 \text{ }^\circ\text{C}$.

Meteorological data are usually measured in UTC (Universal Time Coordinated) or in local time; however, for radiation measurements the mean or, even better, the true local time is desirable. Then, the sun is at its zenith at 12:00 true local time.

Table 1.3 Infrared emissivity of different surfaces (Geiger et al. 2009)

Surface	Emissivity
Water	0.960
Fresh snow	0.986
Coniferous needles	0.971
Dry fine sand	0.949
Wet fine sand	0.962
Thick green grass	0.986

Appendix A.4 gives the necessary calculations and astronomical relations to determine true local time.

Measurements of global radiation are often available in meteorological networks, but other radiation components may be missing. Parameterizations of these missing components using available measurements can be helpful. However, it should be noted that such parameterizations are often based on climatological mean values, and are valid only for the places where they were developed. Their use for short-time measurements is invalid. Jiang et al. (2015) give an overview of how to calculate the net radiation only from data of the global radiation and some additional information.

The possibility to parameterize radiation fluxes using cloud observations was proposed by Burridge and Gadd (1977). For shortwave radiation fluxes, the transmissivity of the atmosphere is used:

$$T_K = (0.6 + 0.2 \sin \Psi)(1 - 0.4 \sigma_{c_H})(1 - 0.7 \sigma_{c_M})(1 - 0.4 \sigma_{c_L}) \quad (1.5)$$

For solar elevation angles $\Psi = 90^\circ$, the transmission coefficient, T_K , ranges from 0.8 to 0.086. σ_c is the cloud cover (0.0–1.0) of high clouds, c_H , of middle clouds, c_M , and c_L of low clouds, (see Supplement 1.3). Please note, that in meteorology the cloud cover is given in octas. (An octa is a fraction equal to one-eighth of the sky.) The incoming shortwave radiation can be calculated using the solar constant S :

$$K \downarrow = \begin{cases} S T_K \sin \Psi, & \Psi \geq 0 \\ 0, & \Psi \leq 0 \end{cases} \quad (1.6)$$

Supplement 1.3 Cloud genera

The classification of clouds is made according their genera and typical height. In the middle latitudes, high clouds are at 5–13 km a.g.l.; middle high clouds at 2–7 km a.g.l., and low clouds at 0–2 km a.g.l. The cloud heights in Polar Regions are lower while in tropical regions clouds heights can be up to 18 km.

Cloud genera	Height	Description
Cirrus (Ci)	High	White, fibrously ice cloud
Cirrocumulus (Cc)	High	Small ice cloud, small fleecy cloud
Cirrostratus (Cs)	High	White stratified ice cloud, halo
Alto cumulus (Ac)	Mean	Large fleecy cloud
Altostratus (As)	Mean	White-grey stratified cloud, ring
Nimbostratus (Ns)	Low	Dark rain/snow cloud
Stratocumulus (Sc)	Low	Grey un-uniform stratified cloud
Stratus (St)	Low	Grey uniform stratified cloud
Cumulus (Cu)	Low ^a –mean	Cumulus cloud
Cumulonimbus (Cb)	Low ^a –high	Thundercloud, anvil cloud

^ain parameterizations classified as low clouds

The reflected shortwave radiation can be calculated according to Eq. (1.3) by using typical values of the albedo of the underlying surface (Table 1.2). The longwave radiation balance can be parameterized using the cloud cover:

$$I^* = I \uparrow + I \downarrow = (0.08 \text{ Kms}^{-1}) \left(1 - 0.1 \sigma_{cH} - 0.3 \sigma_{cM} - 0.6 \sigma_{cL} \right) \quad (1.7)$$

If the surface temperature is given, then the longwave up-welling radiation can be calculated using the Stefan-Boltzmann law, Eq. (1.4). The longwave down-welling radiation can be calculated using Eqs. (1.4) and (1.7).

More often, parameterizations use the duration of sunshine because it was measured for a long time in agricultural networks. Note that time series of sunshine durations are often inhomogeneous because the older Campbell-Stokes sunshine autograph was replaced by electronic methods. These parameterizations are based on climatological cloud structures and can be used only for monthly and annual averaged values, and in the region where the parameterization was developed. The parameterization is based on the well-known Ångström equation with sunshine duration, Sd :

$$K \downarrow = K \downarrow_{\text{extr}} [a + b(Sd/Sd_0)], \quad (1.8)$$

where constants a and b depend on the place of determination. For the German low lands, the constants are, for example, $a \sim 0.19$ and $b \sim 0.55$ (Wendling et al. 1997). The mean daily extraterrestrial incoming irradiation at the upper edge of the atmosphere can be calculated in Wm^{-2} according to:

$$K \downarrow_{\text{extr}} = 28.2[9.9 + 7.08 \zeta + 0.18(\zeta - 1)(\varphi - 51^\circ)] \quad (1.9)$$

This equation is given in a form such that for a geographical latitude of $\varphi = 51^\circ$ no correction for the latitude is necessary. The theoretical sunshine duration is the time between sunrise and sunset and can be expressed in hours

$$Sd_0 = 12.3 + 4.3 \zeta + 0.167 \zeta (\varphi - 51), \quad (1.10)$$

with ($DOY = \text{day of the year}$)

$$\zeta = \sin [DOY (2\pi/365) - 1.39]. \quad (1.11)$$

Because direct measurements of the radiation components are now available, parameterizations should only be used for calculations with historical data.

1.4.2 Ground Heat Flux and Ground Heat Storage

The ground surface (including plants and urban areas) is heated during the day by the incoming shortwave radiation. During the night, the surface cools due to longwave up-welling radiation, and is cooler than the air and the deeper soil layers. High

gradients of temperature are observed in layers only a few millimetres thick (see Sect. 1.3). The energy surplus according to the net radiation is compensated by the turbulent sensible and latent heat fluxes and the mainly molecular ground heat flux. For the generation of latent heat flux, an energy surplus at the ground surface is necessary, and water must be transported through the capillaries and pores of the soil. Energy for the evaporation can also be provided by the soil heat flux in the upper soil layer.

In meteorology, the soil and the ground heat fluxes are often described in a very simple way, e.g. the large differences in the scales in the atmosphere and the soil are often not taken into account. The heterogeneity of soil properties in the scale of 10^{-3} – 10^{-2} m is ignored, and the soil is assumed to be nearly homogeneous for the given meteorological scale. For more detailed investigations, soil physics textbooks must be consulted. In the following, convective heat fluxes and latent heat fluxes in large pores are ignored, because these are measured as sensible and latent heat flux in the atmosphere.

The ground heat flux, Q_G , is based mainly on molecular heat transfer and is proportional to the temperature gradient times the thermal molecular conductivity a_G (Table 1.4):

$$Q_G = a_G \frac{\partial T}{\partial z} \quad (1.12)$$

This molecular heat transfer is so weak that during the day only the upper decimetres are heated. When considering the annual cycle of ground temperature, maximum temperature is at the surface during the summer, but 10–15 m below the surface during winter (Lehmann and Kalb 1993). On a summer day, the ground heat flux is about 50–100 W m^{-2} . A simple but not reliable calculation (Liebethal and Foken 2007) is: $Q_G = -0.1 Q_s^*$ or $Q_G = 0.3 Q_H$ (Stull 1988).

The determination of the ground heat flux according to Eq. (1.12) is not practicable because the temperature profile must be extrapolated to the surface to determine the partial derivative there. This can be uncertain because of the high temperature gradients near the surface (Fig. 1.9) and the difficulties in the determining thermal heat conductivity.

Table 1.4 Thermal molecular conductivity a_G , volumetric heat capacity C_G , and molecular thermal diffusivity ν_T for different soil and ground properties (Stull 1988)

Ground surface	a_G in $\text{W m}^{-1} \text{K}^{-1}$	C_G in $10^6 \text{ W s m}^{-3} \text{K}^{-1}$	ν_T in $10^{-6} \text{ m}^2 \text{s}^{-1}$
Rocks (granite)	2.73	2.13	1.28
Moist sand (40%)	2.51	2.76	0.91
Dry sand	0.30	1.24	0.24
Sandy clay (15%)	0.92	2.42	0.38
Swamp (90% water)	0.89	3.89	0.23
Old snow	0.34	0.84	0.40
New snow	0.02	0.21	0.10

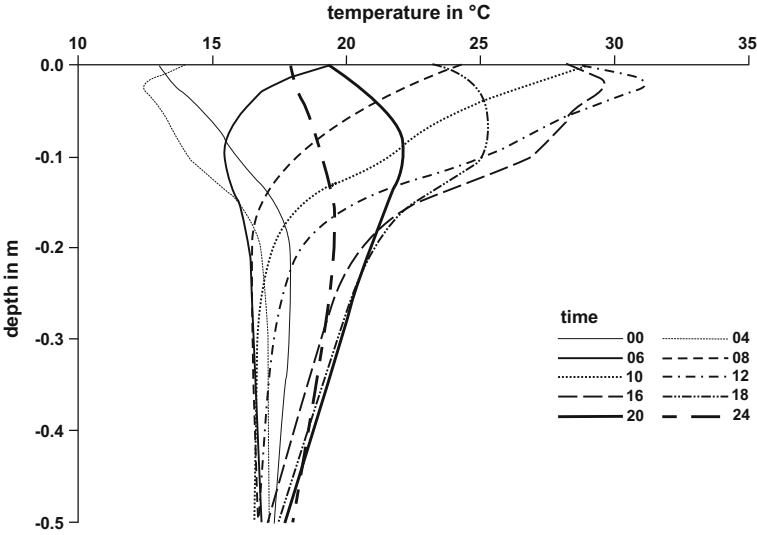


Fig. 1.9 Temperature profile in the upper soil layer on June 05, 1998, measured by the University of Bayreuth during the LITFASS-98 experiment (bare soil) at the boundary layer measuring field site of the Meteorological Observatory Lindenberg (high clouds from 12:00 to 14:00)

However, the ground heat flux at the surface can be estimated as the sum of the soil heat flux measured at some depth using soil heat flux-plates (see Sect. 6.2.6) and the heat storage in the layer between the surface and the plate:

$$Q_G(0) = Q_G(-z) + \int_{-z}^0 \frac{\partial}{\partial t} C_G(z) T(z) dz \quad (1.13)$$

An optimal design for ground heat flux measurements was developed by Liebenthal et al. (2005) using sensitivity analysis. According to their method, the soil heat-flux plate should be buried rather deeply (10–20 cm) with several temperature measurements made above it to calculate the heat storage. A similar accuracy can be achieved if only one temperature profile is measured to calculate both the soil heat flux according to Eq. (1.12) over the depth of 10–20 cm and the heat storage term above this layer and the surface.

The volumetric heat capacity $C_G = a_G/v_T$ (v_T is the molecular thermal diffusivity, Table 1.4), can be assumed constant with depth in the case of uniform soil moisture. A general measurement and calculation guide for the integral of the change of the soil temperature with time is not available. Most institutes have their own schemes, not all of which are optimal solutions. The simplest method is the measurement with an integrating temperature sensor of the mean temperature of the soil layer between the surface and the heat-flux plate. For the ground heat flux near the surface, it then follows that:

$$Q_G(0) = Q_G(-z) + \frac{C_G |\Delta z| \left[\overline{T(t_2)} - \overline{T(t_1)} \right]}{t_2 - t_1} \quad (1.14)$$

The change of the soil temperature with the time can be determined from the vertical gradient of the soil heat flux and using of Eq. (1.12):

$$\frac{\partial T}{\partial t} = \frac{1}{C_G} \frac{\partial Q_G}{\partial z} = v_T \frac{\partial^2 T}{\partial z^2} \quad (1.15)$$

The daily cycle of the soil temperature is to first-order a sine function (Fig. 1.10). Therefore, the surface temperature T_s can be calculated depending on a temperature T_M , which is not affected by the daily cycle, i.e.

$$T_s = T_M + A_s \sin \left[\left(\frac{2\pi}{P} \right) (t - t_M) \right], \quad (1.16)$$

where A_s is the amplitude and P is the period of the wave of the surface temperature and t_M is the time required for $T_s = T_M$ (Arya 2001).

Multiple layers are used for the modelling of the ground heat flux. Because during the daily cycle only the upper soil layers are heated (Fig. 1.10), the two-layer model (force-restore method) developed by Blackadar (1976) is widely used. The ground heat flux can be calculated from two components, i.e., from the change of the temperature of the thin surface layer due to radiation and from the slow wave of the temperature difference between the surface layer and a deeper layer. The equation for the ground heat flux is (Stull 1988):

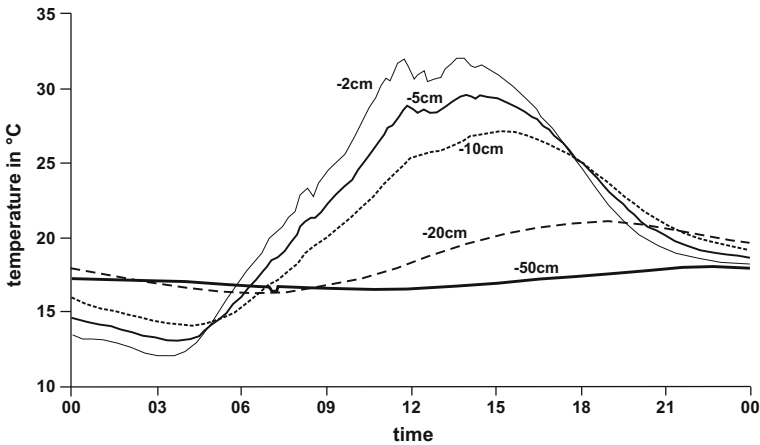


Fig. 1.10 Daily cycle of soil temperatures at different depth on June 05, 1998, measured by the University of Bayreuth during the LITFASS-98 experiment (bare soil) at the boundary layer measuring field site of the Meteorological Observatory Lindenberg (high clouds from 12:00 to 14:00)

$$Q_G = z_G C_G \frac{\partial T_G}{\partial t} + \left(2\pi \frac{z_G C_G}{P} \right) (T_G - T_M), \quad (1.17)$$

where, T_G is the temperature of the upper soil layer, T_M is the temperature of the deeper soil layer, P is the time of the day, and z_G is the thickness of the surface layer. According to Blackadar (1976), $2\pi/P$ is $3 \cdot 10^{-4} \text{ s}^{-1}$ during the day, and $1 \cdot 10^{-4} \text{ s}^{-1}$ at night (day: $T_a < T_G$, night: $T_a > T_G$, T_a : air temperature). The thickness of the upper soil layer depends on the depth of the daily temperature wave:

$$z_G = \sqrt{\frac{v_T P}{4\pi}} \quad (1.18)$$

This can be derived from Eq. (1.15) using Eq. (1.16), see Arya (2001). The force-restore method has the best results in comparison to other parameterization methods (Liebethal and Foken 2007).

1.4.3 Turbulent Fluxes

Contrary to the molecular heat exchange in the soil, heat exchange in the air due to turbulence is much more effective. This is because turbulent exchange occurs over scales of motions ranging from millimetres to kilometres. Turbulent elements can be thought of as air parcels with largely uniform thermodynamic characteristics. Small-scale turbulence elements join to form larger ones and so on. The largest eddies are atmospheric pressure systems. The heated turbulent elements transport their energy by their random motion. This process applies also for trace gases such as water vapour and kinetic energy. The larger turbulent elements receive their energy from the mean motion, and deliver the energy by a cascade process to smaller elements (Fig. 1.11). Small turbulent elements disappear by releasing energy in form of heat (energy dissipation). On average, the transformation of kinetic energy into heat is about 2 Wm^{-2} , which is very small and not considered in the energy balance equation. The reason for this very effective exchange process, which is about a factor of 10^5 greater than the molecular exchange, is the atmospheric turbulence.

Atmospheric turbulence is a specific feature of atmospheric flows with air parcels (turbulent elements or turbulent eddies that are much larger than molecules:) moving irregularly and randomly around a mean state. The length and time scales of these motions cover wide ranges from centimetres and seconds to thousands of kilometres and days.

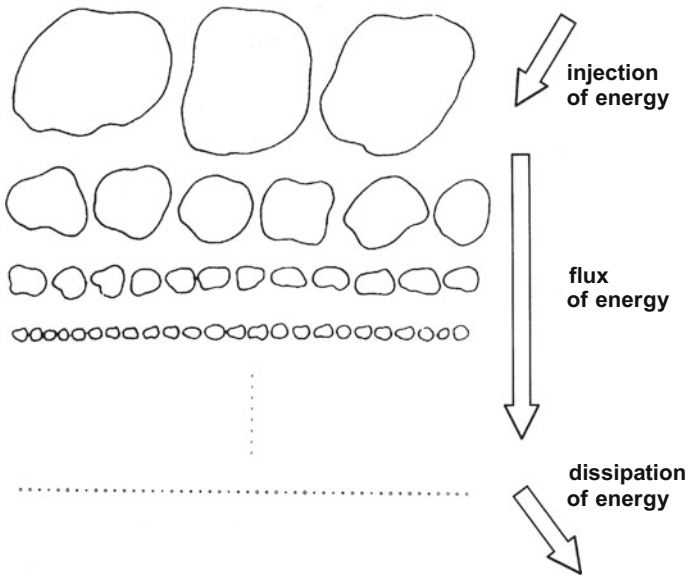


Fig. 1.11 Cascade process of turbulent elements (Frisch 1995), please note that the diminishing of the sizes of the elements is continuous (With kind permission of © Cambridge University Press Cambridge 1995, All rights reserved)

The characteristic distribution of turbulent elements (turbulent eddies) takes place according to their size and is represented by the turbulence spectrum:

The turbulence spectrum describes the energy distribution of turbulent elements (turbulent eddies) according to their wavelength or frequency. Depending on the frequency, the distribution is classified as macro-, meso- or micro turbulence.

The division of atmospheric turbulence occurs over three time ranges, i.e. changes of high and low pressure systems within 3–6 days; the daily cycle of meteorological elements, and the transport of energy, momentum, and trace gases at frequencies ranging from 0.0001 to 10 Hz (Fig. 1.12). The transport of energy and trace gases is the main issue of micrometeorology.

Of special importance, is the inertial sub-range, which is characterized by isotropic turbulence and a constant decrease of the energy density with increasing frequency. In the range from about 0.01–5 Hz, no dominant direction exists for the motion of turbulent elements. The decrease of energy by the decay of larger

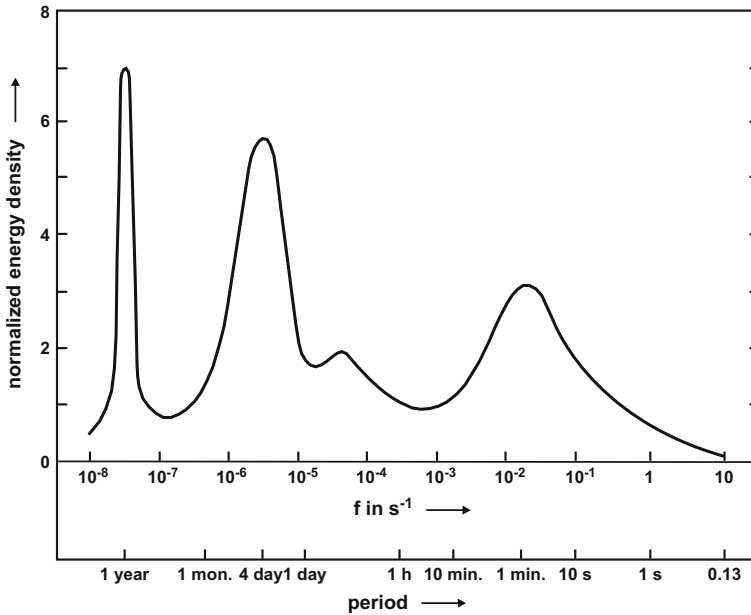


Fig. 1.12 Schematic plot of the turbulence spectra (adaptiert from Roedel and Wagner 2011 with kind permission of © Springer Verlag, Berlin Heidelberg 2000, All rights reserved); the range of frequencies $> 10^{-3}$ Hz is called micro-turbulence, macro-turbulence is from 10^{-6} to 10^{-5} Hz. Between 10^{-5} and 10^{-3} Hz is the range of low energy, the meso-turbulence, and the daily cycle

turbulent elements into smaller ones takes place in a well-defined way according to Kolmogorov's *-5/3-law* (Kolmogorov 1941b). This law predicts that the energy density decreases by five decades when the frequency increases by three decades. The inertial sub-range merges into the dissipation range at the *Kolmogorov's microscale*. The shape of the turbulence spectra depends on the meteorological parameters, the thermal stratification, the height above the ground surface, and the wind velocity (see Sect. 2.5).

A typical property of turbulence, especially in the inertial sub-range, is that turbulent elements change little as they move with the mean flow. Thus, at two neighbouring downwind measuring points the same turbulent structure can be observed at different times. This means that a high autocorrelation of the turbulent fluctuations exists. This is called *frozen turbulence* according to Taylor (1938).

Furthermore, the length scales of turbulent elements increase with the height above the ground surface. In an analogous way, the smallest turbulent elements with the highest frequencies are found near the ground surface. From these findings, it is reasonable to plot the turbulence spectra not as a function of frequency f , but as a dimensionless frequency, n , normalized with the wind speed u and the height z :

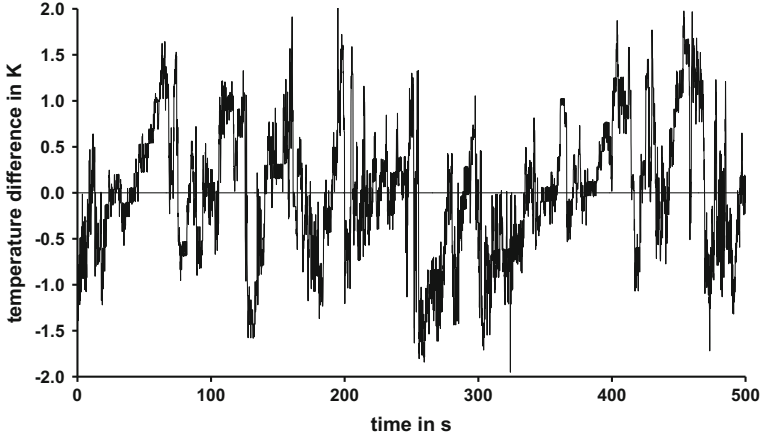


Fig. 1.13 Time series of the air temperature above a spruce forest (University of Bayreuth, Waldstein-Weidenbrunnen site), Aug. 19, 1999, 11:51–12:00 UTC, 500 s measuring period (Wichura et al. 2001)

$$n = f \frac{z}{u} \quad (1.19)$$

(In the English literature, one often sees n as the frequency and f as the dimensionless frequency.)

Turbulent elements can be easily seen, e.g., in plots of temperature time series with high time resolution. In Fig. 1.13, we see short-period disturbances with different intensities superposed onto longer-period (~ 60 s) disturbances. We also see that even significantly larger structures are present.

In analogy to the molecular transport equations (Eq. 1.12), the turbulent heat fluxes (sensible and latent) are often calculated using the vertical gradients of temperature T and specific humidity q (see Supplement 2.2), respectively. However, the molecular transfer coefficients must be replaced by the turbulent diffusion coefficients. The sensible heat flux, Q_H , describes the turbulent transport of heat from and to the earth's surface. The latent heat flux, Q_E , describes the vertical transport of water vapour and the heat required for evaporation at the ground surface. This heat will be deposited later in the atmosphere when condensation occurs, e.g. in clouds. The relevant equations are:

$$Q_H = -\rho c_p K_H \frac{\partial T}{\partial z}, \quad (1.20)$$

$$Q_E = -\rho \lambda K_E \frac{\partial q}{\partial z} \quad (1.21)$$

with the air density ρ , the specific heat for constant pressure c_p , and evaporation heat of water λ . The turbulent diffusion coefficients K_H and K_E are normally complicated functions of the wind speed, the stratification, and the properties of the underlying surface. Their evaluation is a special issue of micrometeorology. In Sect. 2.3, several possible calculations of the diffusion coefficients are discussed. Also common is the *Austausch coefficient* (Schmidt 1925), which is the product of the diffusion coefficient and the air density:

$$A = \rho K \quad (1.22)$$

A typical example of the daily cycle of the turbulent fluxes of two neighbouring surfaces, where one is bare soil and the other covered with barley, is shown in Fig. 1.14. It is obvious that during the night all fluxes have the opposite sign than during the day, and the absolute values are much smaller at night. After sunrise, the signs change and the turbulent fluxes increase rapidly. The time shift between the irradiation and the beginning of turbulence is only a few minutes (Foken et al. 2001). The time shift of the ground heat flux (not shown here) depends on the depth of the soil layer. The maximum of the turbulent fluxes on clear days occurs shortly after midday. Optimal conditions for evaporation are available on the vegetated site, i.e. high soil moisture and strong winds. The sensible heat flux may become negative 1–3 h before sunset, or sometimes shortly after noon, if the radiative fluxes cannot balance the latent heat flux. This phenomenon is called the “oasis effect”, and is also found in temperate latitudes. The latent heat flux, on the other hand, remains large after sunset, until it changes its sign after midnight (dewfall). In contrary, an oasis effect is not prominent on the bare soil (Fig. 1.14), because it dries out during the day and not enough water is available for evaporation.

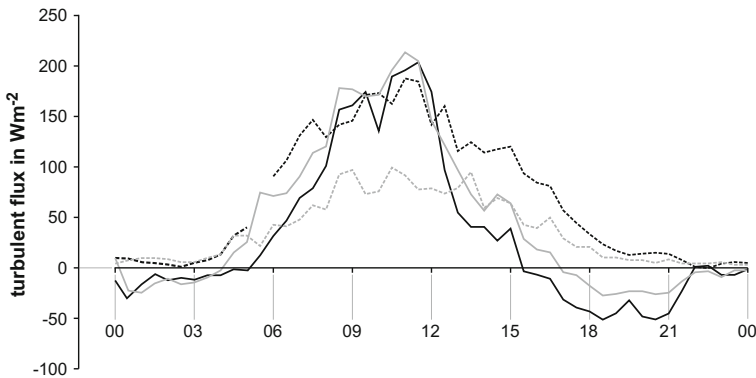


Fig. 1.14 Typical daily cycle of the sensible heat flux (*full line*) and the latent heat flux (*dashed line*) above a barley field (*black lines*) and bare soil (*grey lines*), both fields in a distance of 100 m on June 04, 2003 during the experiment LITFASS-2003

If the sum of all energy fluxes is plotted (Figs. 1.7 and 1.8) it becomes obvious that the energy balance according to Eq. (1.1) is typically not closed when measured data are analysed. This very complex problem is discussed in Sect. 3.7.

While over land in the temperate latitudes the sensible and latent heat fluxes are of the same order, over the ocean the evaporation is much greater. In some climate regions and under extreme weather conditions, significant deviations are possible (Table 1.1).

1.5 Water Balance Equation

The energy balance Eq. (1.1) is connected to the evaporation through the water balance equation:

$$0 = N - Q_E - A \pm \Delta S_W, \quad (1.23)$$

where N is the precipitation, A the runoff, and ΔS_W the sum of the water storage in the soil and ground water. Evaporation is often divided into the physically-caused part, the *evaporation*, which is dependent on the availability of water, the energy input, and the intensity of the turbulent exchange process; and the *transpiration* which is caused by plant-physiology, the water vapour saturation deficit, and the photosynthetic active radiation. The sum of both forms is called *evapotranspiration*. Evaporation occurs on the ground, on water surfaces, and on wetted plant surfaces. The latter is the evaporation of precipitation water held back at plant surfaces (interception). Micrometeorology plays an important role for the determination of evapotranspiration and the investigation of the water cycle (Table 1.5). Data show that the precipitation–evaporation cycle over the land is not as strongly coupled as they are over the ocean. This means that precipitation is mainly generated over regions where water evaporated.

The water balance equation is widely used in hydrological investigations. Thus, evaporation connects meteorology with hydrology. This field of investigations is often called hydrometeorology.

Table 1.5 Water cycle of the earth in $10^3 \text{ km}^3 \text{ a}^{-1}$ (Brutsaert 2005, modified and updated)

Reference	N	Q_E	N	Q_E	Transport
	<i>Above land</i>		<i>Above ocean</i>		<i>Ocean–land</i>
Budyko (1974)	109	63	412	455	46
Baumgartner and Reichel (1975)	112	72	386	426	40
Korzun (1978)	119	72	458	505	47
Houghton (2015)	111	71	385	425	40

References

- Albrecht F (1940) Untersuchungen über den Wärmehaushalt der Erdoberfläche in verschiedenen Klimagebieten. Reichsamt Wetterdienst, Wiss Abh. Bd. VIII, Nr. 2:1–82.
- André J-C, Bougeault P and Goutorbe J-P (1990) Regional estimates of heat and evaporation fluxes over non-homogeneous terrain, Examples from the HAPEX-MOBILHY programme. *Boundary-Layer Meteorol.* 50:77–108.
- Arya SP (2001) *Introduction to Micrometeorology*. Academic Press, San Diego, 415 pp.
- Barkov E (1914) Vorläufiger Bericht über die meteorologischen Beobachtungen der Deutschen Antarktisexpedition 1911–1912. *Meteorol Z.* 49:120–126.
- Barrett EW and Suomi VE (1949) Preliminary report on temperature measurement by sonic means. *J Meteorol.* 6:273–276.
- Baumgartner A and Reichel E (1975) *The World Water Balance*. Elsevier, Amsterdam, New York, 179 pp.
- Beniston M (1998) *From Turbulence to Climate*. Springer, Berlin, Heidelberg, 328 pp.
- Beyrich F and Mengelkamp H-T (2006) Evaporation over a heterogeneous land surface: EVA_GRIPS and the LITFASS-2003 experiment - an overview. *Boundary-Layer Meteorol.* 121:5–32.
- Bird RB, Stewart WE and Lightfoot EN (2007) *Transport Phenomena*. John Wiley & Sons, Inc., New York, 905 pp.
- Blackadar AK (1976) Modeling the nocturnal boundary layer. 4th Symposium on Atmospheric Turbulence, Diffusion and Air Pollution, Raylaigh, NC, Oct. 19–22, 1976. *Am. Meteorol. Soc.*, pp. 46–49.
- Blöschl G and Sivapalan M (1995) Scale issues in hydrological modelling - a review. *Hydrol Processes.* 9:251–290.
- Bovsheverov VM and Voronov VP (1960) Akustitscheskii fljuzer (Acoustic rotor). *Izv AN SSSR, ser Geofiz.* 6:882–885.
- Bradley EF (1968) A shearing stress meter for micrometeorological studies. *Quart J Roy Meteorol Soc.* 94:380–387.
- Brutsaert W (2005) *Hydrology*. Cambridge University Press, Cambridge, XII, 605 pp.
- Budyko MI (1974) *Climate and Life*. Academic Press, New York, 508 pp.
- Burridge DM and Gadd AJ (1977) The Meteorological Office operational 10-level numerical weather prediction model (December 1975). *Meteorological Office Technical Notes.* 34:39 pp.
- Businger JA and Yaglom AM (1971) Introduction to Obukhov's paper "Turbulence in an atmosphere with a non-uniform temperature". *Boundary-Layer Meteorol.* 2:3–6.
- Businger JA, Wyngaard JC, Izumi Y and Bradley EF (1971) Flux-profile relationships in the atmospheric surface layer. *J Atmos Sci.* 28:181–189.
- Davidson PA, Kaneda Y, Moffatt K and Sreenivasan KR (eds) (2011) *A Voyage through Turbulence*. Cambridge University Press, Cambridge, 434 pp.
- Dutton JA (2002) *The Ceaseless Wind: An Introduction to the Theory of Atmospheric Motion*. Dover Publications, Mineola, NY, 640 pp.
- Dyer AJ, Hicks BB and King KM (1967) The Fluxatron - A revised approach to the measurement of eddy fluxes in the lower atmosphere. *Journal Applied Meteorology.* 6:408–413.
- Dyer AJ, Garratt JR, Francey RJ, McIlroy IC, Bacon NE, Hyson P, Bradley EF, Denmead DT, Tsvang LR, Volkov JA, Kaprov BM, Elagina LG, Sahashi K, Monji N, Hanafusa T, Tsukamoto O, Frenzen P, Hicks BB, Wesely M, Miyake M and Shaw WJ (1982) An international turbulence comparison experiment (ITCE 1976). *Boundary-Layer Meteorol.* 24:181–209.
- Etling D (2008) *Theoretische Meteorologie*. Springer, Berlin, Heidelberg, 376 pp.
- Foken T, Kitajgorodskij SA and Kuznecov OA (1978) On the dynamics of the molecular temperature boundary layer above the sea. *Boundary-Layer Meteorol.* 15:289–300.

- Foken T, Wichura B, Klemm O, Gerchau J, Winterhalter M and Weidinger T (2001) Micrometeorological conditions during the total solar eclipse of August 11,1999. *Meteorol Z.* 10:171–178.
- Foken T (2006) 50 years of the Monin-Obukhov similarity theory. *Boundary-Layer Meteorol.* 119:431–447.
- Foken T, Meixner FX, Falge E, Zetzsch C, Serafimovich A, Bargsten A, Behrendt T, Biermann T, Breuninger C, Dix S, Gerken T, Hunner M, Lehmann-Pape L, Hens K, Jocher G, Kesselmeier J, Lüers J, Mayer JC, Moravek A, Plake D, Riederer M, Rütz F, Scheibe M, Siebicke L, Sörgel M, Staudt K, Trebs I, Tsokankunku A, Welling M, Wolff V and Zhu Z (2012) Coupling processes and exchange of energy and reactive and non-reactive trace gases at a forest site – results of the EGER experiment. *Atmos Chem Phys.* 12:1923–1950.
- Foken T (2013) *Energieaustausch an der Erdoberfläche.* Edition am Gutenbergplatz, Leipzig, 99 pp.
- Frisch U (1995) *Turbulence.* Cambridge Univ. Press, Cambridge, 296 pp.
- Garratt JR (1978) Flux profile relations above tall vegetation. *Quart J Roy Meteorol Soc.* 104:199–211.
- Garratt JR and Hicks BB (1990) Micrometeorological and PBL experiments in Australia. *Boundary-Layer Meteorol.* 50:11–32.
- Garratt JR (1992) *The Atmospheric Boundary Layer.* Cambridge University Press, Cambridge, 316 pp.
- Geiger R (1927) *Das Klima der bodennahen Luftschicht.* Friedr. Vieweg & Sohn, Braunschweig, 246 pp.
- Geiger R, Aron RH and Todhunter P (2009) *The Climate near the Ground.* Rowman & Littlefield, Lanham, XVIII, 623 pp.
- Geiger R (2013) *Das Klima der bodennahen Luftschicht.* Springer Vieweg, Wiesbaden, 646 pp.
- Glickman TS (ed) (2000) *Glossary of Meteorology.* Am. Meteorol. Soc., Boston, MA, 855 pp.
- Hanafusa T, Fujitana T, Kobori Y and Mitsuta Y (1982) A new type sonic anemometer-thermometer for field operation. *Papers Meteorol Geophys.* 33:1–19.
- Hann JF and Stüring R (1939) *Lehrbuch der Meteorologie.* Verlag von Willibald Keller, Leipzig, 480 pp.
- Hartmann DL (1994) *Global Physical Climatology.* Academic Press, San Diego, New York, 408 pp.
- Haugen DA (ed) (1973) *Workshop on Micrometeorology.* Am. Meteorol. Soc., Boston, 392 pp.
- Henderson-Sellers A and Robinson PJ (1986) *Contemporary Climatology.* John Wiley & Sons, Inc., New York, 439 pp.
- Högström U (1988) Non-dimensional wind and temperature profiles in the atmospheric surface layer: A re-evaluation. *Boundary-Layer Meteorol.* 42:55–78.
- Högström U (1990) Analysis of turbulence structure in the surface layer with a modified similarity formulation for near neutral conditions. *J Atmos Sci.* 47:1949–1972.
- Houghton DD (1985) *Handbook of applied meteorology.* Wiley, New York, XV, 1461 pp.
- Houghton JT (2015) *Global Warming, The complete Briefing.* Cambridge University Press, Cambridge, 396 pp.
- Hupfer P and Kuttler W (eds) (2005) *Witterung und Klima, begründet von Ernst Heyer.* B.G. Teubner, Stuttgart, Leipzig, 554 pp.
- Izumi Y (1971) *Kansas 1968 field program data report.* Air Force Cambridge Research Laboratory, Bedford, MA, 79 pp.
- Jiang B, Zhang Y, Liang S, Wohlfahrt G, Arain A, Cescatti A, Georgiadis T, Jia K, Kiely G, Lund M, Montagnani L, Magliulo V, Ortiz PS, Oechel W, Vaccari FP, Yao Y and Zhang X (2015) Empirical estimation of daytime net radiation from shortwave radiation and ancillary information. *Agrical Forest Meteorol.* 211–212:23–36.
- Kaimal JC and Businger JA (1963) A continuous wave sonic anemometer-thermometer. *J Climate Appl Meteorol* 2:156–164.

- Kaimal JC and Wyngaard JC (1990) The Kansas and Minnesota experiments. *Boundary-Layer Meteorol.* 50:31–47.
- Kiehl J and Trenberth KE (1997) Earth annual global mean energy budget. *Bull Amer Meteorol Soc.* 78:197–208.
- Kleinschmidt E (ed) (1935) *Handbuch der meteorologischen Instrumente und ihrer Auswertung.* Springer, Berlin, 733 pp.
- Kolmogorov AN (1941a) Lokalnaja struktura turbulentnosti v neschtschimaemoi schidkosti pri otschen bolschich tschislach Reynoldsa (The local structure of turbulence in incompressible viscous fluid for very large Reynolds numbers). *Dokl AN SSSR.* 30:299–303.
- Kolmogorov AN (1941b) Rassejanie energii pri lokalno-isotropoi turbulentnosti (Dissipation of energy in locally isotropic turbulence). *Dokl AN SSSR.* 32:22–24.
- Kopp G and Lean JL (2011) A new, lower value of total solar irradiance: Evidence and climate significance. *Geophys Res Letters.* 38:L01706.
- Korzun VI (ed) (1978) *World Water Balance and Water Resources of the Earth.* UNESCO, Paris, 663 pp.
- Kraus H (2004) *Die Atmosphäre der Erde.* Springer, Berlin, Heidelberg, 422 pp.
- Kraus H (2008) *Grundlagen der Grenzschichtmeteorologie.* Springer, Berlin, Heidelberg, 211 pp.
- Lehmann A and Kalb M (1993) 100 Jahre meteorologische Beobachtungen an der Säkularstation Potsdam 1893–1992. *Deutscher Wetterdienst, Offenbach,* 32 pp.
- Lettau H (1939) *Atmosphärische Turbulenz.* Akad. Verlagsges., Leipzig, 283 pp.
- Lettau H (1949) Isotropic and non-isotropic turbulence in the atmospheric surface layer. *Geophys Res Pap.* 1:86 pp.
- Lettau HH and Davidson B (eds) (1957) *Exploring the Atmosphere's First Mile.* Pergamon Press, London, New York, 376 pp.
- Liebenthal C, Huwe B and Foken T (2005) Sensitivity analysis for two ground heat flux calculation approaches. *Agrical Forest Meteorol.* 132:253–262.
- Liebenthal C and Foken T (2007) Evaluation of six parameterization approaches for the ground heat flux. *Theor Appl Climat.* 88:43–56.
- Liou KN (1992) *Radiation and Cloud Processes in the Atmosphere.* Oxford University Press, Oxford, 487 pp.
- Lothon M, Lohou F, Pino D, Couvreur F, Pardyjak ER, Reuder J, Vilà-Guerau de Arellano J, Durand P, Hartogensis O, Legain D, Augustin P, Gioli B, Lenschow DH, Faloona I, Yagüe C, Alexander DC, Angevine WM, Bargain E, Barrié J, Bazile E, Bezombes Y, Blay-Carreras E, van de Boer A, Boichard JL, Bourdon A, Butet A, Campistron B, de Coster O, Cuxart J, Dabas A, Darbieu C, Deboudt K, Delbarre H, Derrien S, Flament P, Fourmentin M, Garai A, Gibert F, Graf A, Groebner J, Guichard F, Jiménez MA, Jonassen M, van den Kroonenberg A, Magliulo V, Martin S, Martinez D, Mastrorillo L, Moene AF, Molinos F, Moulin E, Pietersen HP, Piguet B, Pique E, Román-Cascón C, Rufin-Soler C, Saïd F, Sastre-Marugán M, Seity Y, Steeneveld GJ, Toscano P, Traullé O, Tzanos D, Wacker S, Wildmann N and Zaldei A (2014) The BLLAST field experiment: Boundary-Layer Late Afternoon and Sunset Turbulence. *Atmos Chem Phys.* 14:10931–10960.
- Lumley JL and Yaglom AM (2001) A century of turbulence. *Flow, Turbulence and Combustion.* 66:241–286.
- Mitsuta Y (1966) Sonic anemometer-thermometer for general use. *J Meteor Soc Japan. Ser. II,* 44:12–24.
- Miyake M, Stewart RW, Burling RW, Tsvang LR, Kaprov BM and Kuznecov OA (1971) Comparison of acoustic instruments in an atmospheric flow over water. *Boundary-Layer Meteorol.* 2:228–245.
- Monin AS and Obukhov AM (1954) Osnovnye zakonomernosti turbulentnogo peremesivaniya v prizemnom sloe atmosfery (Basic laws of turbulent mixing in the atmosphere near the ground). *Trudy geofiz inst AN SSSR.* 24 (151):163–187.

- Monin AS and Yaglom AM (1973) *Statistical Fluid Mechanics: Mechanics of Turbulence*, Volume 1. MIT Press, Cambridge, London, 769 pp.
- Monin AS and Yaglom AM (1975) *Statistical Fluid Mechanics: Mechanics of Turbulence*, Volume 2. MIT Press, Cambridge, London, 874 pp.
- Montgomery RB (1948) Vertical eddy flux of heat in the atmosphere. *Journal Meteorology*. 5:265–274.
- Obukhov AM (1946) Turbulentnost' v temperaturnoj - neodnorodnoj atmosfere (Turbulence in an atmosphere with a non-uniform temperature). *Trudy Inst Theor Geofiz AN SSSR* 1:95–115.
- Obukhov AM (1951) Charakteristiki mikrostrukturny vetra v prizemnom sloje atmosfery (Characteristics of the micro-structure of the wind in the surface layer of the atmosphere). *Izv AN SSSR, ser Geofiz.* 3:49–68.
- Obukhov AM (1960) O strukture temperaturnogo polja i polja skorostej v uslovijach konvekcii (Structure of the temperature and velocity fields under conditions of free convection). *Izv AN SSSR, ser Geofiz.* 9:1392–1396.
- Obukhov AM (1971) Turbulence in an atmosphere with a non-uniform temperature. *Boundary-Layer Meteorol.* 2:7–29.
- Oertel H (ed) (2004) *Prandtl's essentials of fluid mechanics*. Springer, New York, VII, 723 pp.
- Oke TR (1987) *Boundary Layer Climates*. Methuen, New York, 435 pp.
- Onclay SP, Foken T, Vogt R, Kohsiek W, DeBruin HAR, Bernhofer C, Christen A, van Gorsel E, Grantz D, Feigenwinter C, Lehner I, Liebethal C, Liu H, Mauder M, Pitacco A, Ribeiro L and Weidinger T (2007) The energy balance experiment EBEX-2000, Part I: Overview and energy balance. *Boundary-Layer Meteorol.* 123:1–28.
- Orlanski I (1975) A rational subdivision of scales for atmospheric processes. *Bull. Am. Meteorol. Soc.* 56:527–530.
- Persson POG, Fairall CW, Andreas EL, Guest PS and Perovich DK (2002) Measurements near the atmospheric surface flux group tower at sheba: Near-surface conditions and surface energy budget. *J Geophys Res.* 107:8045.
- Poulos GS, Blumen W, Fritts DC, Lundquist JK, Sun J, Burns SP, Nappo C, Banta R, Newsom R, Cuxart J, Terradellas E, Balsley B and Jensen M (2002) CASES-99: A comprehensive investigation of the stable nocturnal boundary layer. *Bull Amer Meteorol Soc.* 83:55–581.
- Prandtl L (1925) Bericht über Untersuchungen zur ausgebildeten Turbulenz. *Z angew Math Mech.* 5:136–139.
- Priestley CHB and Swinbank WC (1947) Vertical transport of heat by turbulence in the atmosphere. *Proceedings Royal Society London.* A189:543–561.
- Reynolds O (1894) On the dynamical theory of turbulent incompressible viscous fluids and the determination of the criterion. *Phil Trans R Soc London.* A 186:123–161.
- Richardson LF (1920) The supply of energy from and to atmospheric eddies. *Proceedings Royal Society.* A 97:354–373.
- Roedel W and Wagner T (2011) *Physik unserer Umwelt: Die Atmosphäre*. Springer, Berlin, Heidelberg pp.
- Schlichting H and Gersten K (2003) *Boundary-Layer Theory*. McGraw Hill, New York, XXIII, 799 pp.
- Schmidt W (1925) *Der Massenaustausch in freier Luft und verwandte Erscheinungen*. Henri Grand Verlag, Hamburg, 118 pp.
- Schoonmaker PK (1998) Paleocological perspectives on ecological scales. In: Peterson DL and Parker VT (eds.), *Ecological Scale*. Columbia University Press, New York, 79–103.
- Schotland RM (1955) The measurement of wind velocity by sonic waves. *J Meteorol.* 12:386–390.
- Seibert P, Beyrich F, Gryning S-E, Joffre S, Rasmussen A and Tercier P (2000) Review and intercomparison of operational methods for the determination of the mixing height. *Atmos Environm.* 34:1001–1027.
- Sellers PJ, Hall FG, Asrar G, Strelbel DE and Murphy RE (1988) The first ISLSCP field experiment (FIFE). *Bull Amer Meteorol Soc.* 69:22–27.

- Shen S and Leclerc MY (1995) How large must surface inhomogeneous be before they influence the convective boundary layer structure? A case study. *Quart J Roy Meteorol Soc.* 121: 1209–1228.
- Stull RB (1988) *An Introduction to Boundary Layer Meteorology*. Kluwer Acad. Publ., Dordrecht, Boston, London, 666 pp.
- Suomi VE (1957) Sonic anemometer - University of Wisconsin. In: Lettau HH and Davidson B (eds.), *Exploring the atmosphere's first mile*, vol 1. Pergamon Press, London, New York, 256–266.
- Sutton OG (1953) *Micrometeorology*. McGraw Hill, New York, 333 pp.
- Swinbank WC (1951) The measurement of vertical transfer of heat and water vapor by eddies in the lower atmosphere. *J Meteorol.* 8:135–145.
- Taylor GI (1915) Eddy motion in the atmosphere. *Phil Trans R Soc London.* A 215:1–26.
- Taylor GI (1938) The spectrum of turbulence. *Proceedings Royal Society London.* A 164: 476–490.
- Trenberth KE, Fasullo JT and Kiehl J (2009) Earth's Global Energy Budget. *Bull Amer Meteorol Soc.* 90:311–323.
- Tsvang LR, Kaprov BM, Zubkovskij SL, Dyer AJ, Hicks BB, Miyake M, Stewart RW and McDonald JW (1973) Comparison of turbulence measurements by different instruments; Tsimlyansk field experiment 1970. *Boundary-Layer Meteorol.* 3:499–521.
- Tsvang LR, Zubkovskij SL, Kader BA, Kallistratova MA, Foken T, Gerstmann W, Przandka Z, Pretel J, Zelený J and Keder J (1985) International turbulence comparison experiment (ITCE-81). *Boundary-Layer Meteorol.* 31:325–348.
- Tsvang LR, Fedorov MM, Kader BA, Zubkovskii SL, Foken T, Richter SH and Zelený J (1991) Turbulent exchange over a surface with chessboard-type inhomogeneities. *Boundary-Layer Meteorol.* 55:141–160.
- Vogel H-J and Roth K (2003) Moving through scales of flow and transport in soil. *J Hydrol.* 272:95–106.
- von Kármán T and Howarth L (1938) On the statistical theory of isotropic turbulence. *Proceedings Royal Society London.* A 164:192–215.
- Wendisch M and Yang P (2012) *Theory of Atmospheric Radiative Transfer*. Wiley & Sons, Inc., Weinheim pp.
- Wendling U, Fuchs P and Müller-Westermeier G (1997) Modellierung des Zusammenhangs von Globalstrahlung, Sonnenscheindauer und Bewölkungsgrad als Beitrag der Klimaüberwachung. *Dt Wetterdienst, Forsch. Entwicklung, Arbeitsergebnisse.* 45:29 pp.
- Wichura B, Buchmann N, Foken T, Mangold A, Heinz G and Rebmann C (2001) Pools und Flüsse des stabilen Kohlenstoffisotops ¹³C zwischen Boden, Vegetation und Atmosphäre in verschiedenen Pflanzengemeinschaften des Fichtelgebirges. *Bayreuther Forum Ökologie.* 84:123–153.
- Wieringa J (1980) A reevaluation of the Kansas mast influence on measurements of stress and cup anemometer overspeeding. *Boundary-Layer Meteorol.* 18:411–430.
- Wild M, Folini D, Schär C, Loeb N, Dutton E and König-Langlo G (2013) The global energy balance from a surface perspective. *Climate Dynamics.* 40:3107–3134.
- Wild M, Folini D, Hakuba M, Schär C, Seneviratne S, Kato S, Rutan D, Ammann C, Wood E and König-Langlo G (2015) The energy balance over land and oceans: an assessment based on direct observations and CMIP5 climate models. *Climate Dynamics.* 44:3393–3429.
- Wulfmeyer V, Behrendt A, Kottmeier C, Corsmeier U, Barthlott C, Craig G, Hagen M, Althausen D, Aoshima F, Arpagaus M, Bauer HS, Bennett L, Blyth A, Brandau C, Champollion C, Crewell S, Dick G, Di Girolamo P, Dorninger M, Dufournet Y, Eigenmann R, Engelmann R, Flamant C, Foken T, Gorgas T, Grzeschik M, Handwerker J, Hauck C, Höller H, Junkermann W, Kalthoff N, Kiemle C, Klink S, König M, Krauß L, Long CN, Madonna F, Mobbs S, Neining B, Pal S, Peters G, Pigeon G, Richard E, Rotach M, Russchenberg H, Schwitala T, Smith V, Steinacker R, Trentmann J, Turner DD, van Baelen J, Vogt S,

- Volkert H, T. W, Wernli H, Wieser A and Wirth M (2011) The convective and orographically induced precipitation study (COPS): The scientific strategy, the field phase, and research highlights. *Quart J Roy Meteorol Soc.* 137:3–30.
- Wyngaard JC, Côté OR and Izumi Y (1971) Local free convection, similarity and the budgets of shear stress and heat flux. *J Atmos Sci.* 28:1171–1182.
- Wyngaard JC, Businger JA, Kaimal JC and Larsen SE (1982) Comments on ‘A reevaluation of the Kansas mast influence on measurements of stress and cup anemometer overspeeding’. *Boundary-Layer Meteorol.* 22:245–250.